• 物理电子学 •

Analysis of Electromagnetic Radiation of Secondary Ion Radiation Induced by Laser Interaction with Solid Target

YI Tao[1*], YANG Yu[1,2], XU Yilin[2], LI Zihao[2], WANG Chuanke[1], and LI Tingshuai[2]

(1. Laser Fusion Research Center, Chinese Academy of Engineering Physics Mianyang Sichuan 621900;
2. School of Materials and Energy, University of Electronic Science and Technology of China Chengdu 611731)

Abstract Significant radiations in the frequencies ranging from gamma rays and X-rays to radio frequency can be generated during the interactions between powerful lasers with solid targets. Gamma rays are able to penetrate metal walls of diagnostic setups and induce secondary electrons, which can further radiate Electromagnetic Pulses (EMPs). In this study, emissions of secondary electrons due to gamma-metal interactions are quantitatively simulated. The results indicate that secondary ions are strongly pertinent to the incident Gamma rays, metal contents and metal shapes. The Maxwell's equations confirm that electromagnetic pulses partially stem from the secondary charges, and its average energy and spatial distribution are also discussed. The resulting conclusions are beneficial to deepen understanding of EMP generations and also offer more experimental supports to achieve an effective shielding design for various physical diagnostics.

Key words electromagnetic pulses; gamma rays; laser; secondary electrons; simulation

激光与固体靶相互作用诱导的次级离子辐射电磁辐射规律分析

易 涛[1*]，杨 雨[1,2]，徐毅麟[2]，李子豪[2]，王传珂[1]，李廷帅[2]

(1. 中国工程物理研究院激光聚变研究中心 四川 绵阳 621900；2. 电子科技大学材料与能源学院 成都 611731)

【摘要】强激光与固体靶相互作用可以产生从伽马射线、X 射线到无线电频率范围内的各类辐射。伽马射线能够穿透诊断装置的金属壁并诱导二次电子，二次电子进一步辐射电磁脉冲 (EMP)。该文定量模拟了由伽马与金属相互作用引起的次级电子发射。结果表明二次离子与入射伽马射线、金属含量和金属形状密切相关。麦克斯韦方程组证实了电磁脉冲部分源于二次电荷，最后讨论了其平均能量和空间分布。研究结果有助于加深对 EMP 产生机制的认识，也为各种物理诊断的有效屏蔽设计提供更多的实验支持。

关 键 词 电磁脉冲； 伽马射线； 激光； 二次电子； 模拟
中图分类号 TL632; O441.4 **文献标志码** A doi:10.12178/1001-0548.2021323

Since high plasma density and temperature are essential to realize thermonuclear reactions, the laser-driven target is one of the viable approaches to achieve ignition and gain with inertial confinement fusion[1-3], which has attracted increasing attentions due to the global energy crises and ever-worsening environment. Several large laser facilities including LMJ[4], National Ignition Facility (NIF)[5] and HiPER[6] are thus designed and constructed over the past decades. Particularly, NIF as the largest laser facility in the world, developed by Lawrence Livermore National Laboratory (LLNL), has achieved a sustainable and reliable output up to a total laser radiation power of 2 500 W[7]. However, there are still challenges such as various radiations that can severely interfere with some critical physical diagnostics and even result in malfunction of diagnostic setups.

When atoms in solid targets are exposed to the

Received date: 2022 − 11 − 05; Revised date: 2023 − 02 − 21
收稿日期：2022 − 11 − 05；修回日期：2023 − 02 − 21
Biography: YI Tao(1980 −), male, phD, his reaserach interests include laser plasmas EMP.
作者简介：易涛 (1980 −)，男，博士，主要从事激光等离子体电磁脉冲方面的研究.
*Corresponding author: YI Tao, E-mail: ylexington@sina.com
*通信作者：易涛，E-mail：ylexington@sina.com

superpower laser field, a large number of photons will be absorbed, which enables the hot electrons to escape from the target surface during the continuous inelastic process [8] and these collisional electrons are heated in the skin layer of metal[9]. Afterwards, the energy absorbed from these photons is transmitted to X-rays, gamma rays, neutrons and electrons[10]. Previous reports indicated that high-energy secondary electrons were found to transmit in the same direction of their parent protons during synchrotron emission. Besides, electromagnetic cascade occurred between these electrons, which led to the generation of gamma rays[11].

Conrad et al. reported that the drift of these secondary electron-ions accounted for the Electromagnetic Pulses (EMPs) generation[12-13]. A significant decline of EMP energy was observed during the change of laser energy, along with a decline of the number of ejected energetic electrons[14]. When the electrical current caused by secondary electrons reached the interface between two different media, EMPs could be generated[15], but differently, the main hot electrons from laser interaction with targets would cause more intensive EMP emissions[5]. Moreover, while metals were not connected to ground, the emission of electrons could directly result in the generation of EMPs[16]. Electromagnetic Interference (EMI) in a laser chamber was closely related to the EMPs, which affected the accuracy of some crucial physical diagnostics inside the laser chambers[5,17-18]. However, since the progress of plasma expansion was extremely complicated, the relationship between EMP signals and gamma rays could hardly be directly described by equations, yet the motion state of secondary electrons had not been quantified during the interactions between gamma rays and metals.

Given the detrimental effects of electromagnetic pulses, the secondary electrons are studied by high-frequency radiations interacting with metals under varying conditions based on the practical experiment obtained from high power laser facility. The relationship between distributions and energy of the secondary ions with laser and metals are investigated. The conclusions drawn in this study are expected to offer a new avenue to detect and analyze EMPs stemming from laser shooting solid targets and helpful to design effective shielding for physical experiments.

1 Experimental Arrangements

Measurements of EMPs were conducted at high power laser facility[19-21]. To precisely evaluate the EMPs ' origins in the large laser facility, secondary ions induced by high-frequency radiations should be taken into account. We have carried out plenty of measurements regarding EMPs inside and outside the laser facility[19,22-24], which can be used to support our simulations concerning steak camera.

A multi-material shield was designed to attenuate EMP, combining 0.1 mm teflon, 2 cm Cu and 2.4 cm lead. Extra shield was used to prevent EMP from being externally coupled into the coaxes line and interconnecting piece. As displayed in Fig. 1, two antenna-oscilloscope systems were used to record EMP signals inside and outside the shielding room when laser beams were incident on the targets. Antennas and diagnostic setups were placed in the Diagnostic Instrument Manipulator (DIM), which was pushed into the target chamber in the experiment.

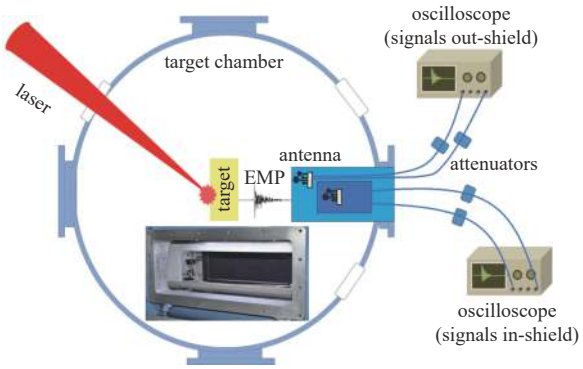

Fig. 1 Schematic experimental arrangement for EMPs' measurement

2 Results and Discussion

EMP signals can be attenuated to undetectable level after effectively shielding, in which teflon, copper and lead are used as shielding materials, as Fig. 2 shows. However, as some case shown in Fig. 3, lower intensity signals are detected inside the shield. The oscillatory signal lasting for 150 ns, suggests that

an oscillation of EMP occurrs. It is worth noting that, the decay rate of EMP signals inside the shield and outside the shield are different. Meanwhile, the frequency of EMP shifts from 0.7～1.4 GHz to 0～0.7 GHz. There must be a new source for EMP inside the shield, which means that the EMP inside the shield contains newly generated component.

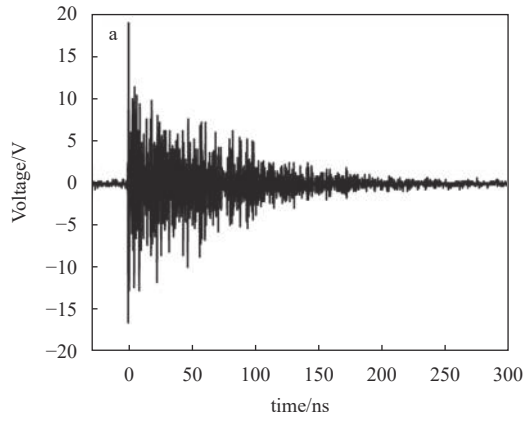

a. without shielding

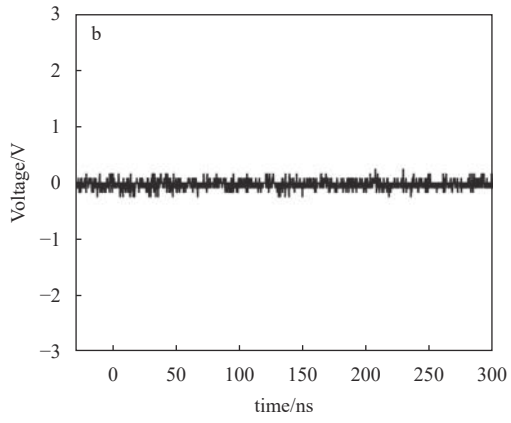

b. with shielding

Fig. 2　EMP signals detected by the probe

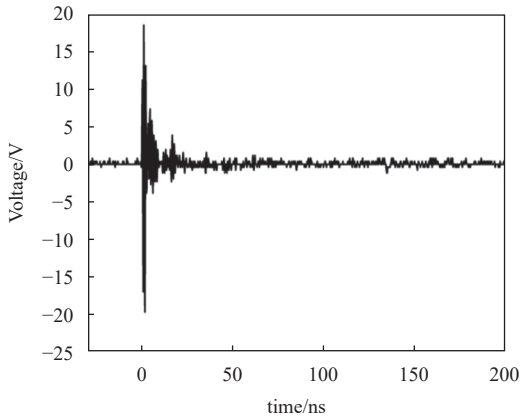

a. outside the shield in time domain

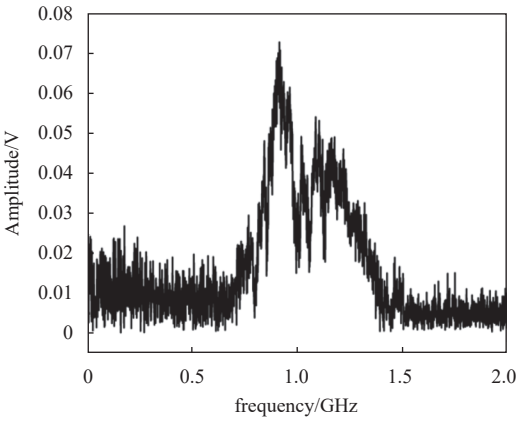

b. outside the shield in frequency domain

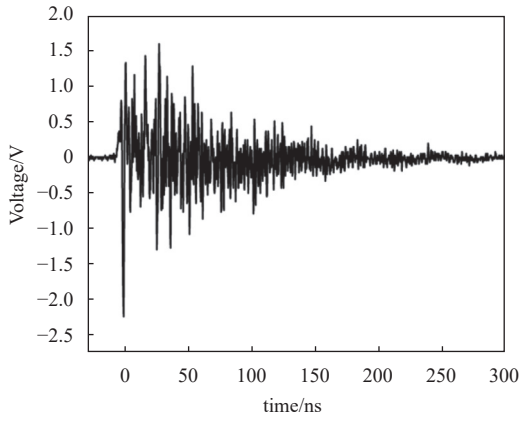

c. inside the shield in time domain

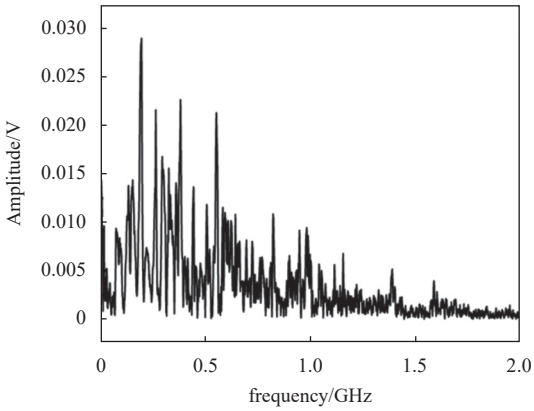

d. inside the shield in frequency domain

Fig. 3　The detected EMP signals and corresponding frequency distributions

The interaction between high-intense photons and targets produces abundant secondary effects, most of which are related to energetic electrons[25]. Meanwhile, according to Maxwell's equations, since the electric field and magnetic field are related to charge particles, a model concerning secondary ions isthus developed using Monte Carlo to thoroughly explore the mechanism of EMPs formation in laser shooting solid

targets.

Note that laser is not directly focused on the shield in our test, EMP signals inside the metal shielding cage are impossible to be directly induced by laser irradiating targets. High-Frequency radiations like gamma rays can be generated during the interaction of laser on solid targets, which possibly stimulates the metal walls of chamber and even metal shielding layer to yield secondary ions, accounting for EMP emerging in the shielding cage. To unravel the process of electron generation due to gamma rays striking metal walls, energy and numbers of hot electrons from the interaction between gamma rays and metals are thus simulated and analysed. As shown in Fig. 4, the metal wall whose normal direction coincides with the z-axis is irradiated by gamma rays whose incident direction is negative along the z-axis. There are seven particle collectors at different azimuth directions, varying from 0 degree to 180 degrees (0 degree means that it coincides with the incident direction of gamma rays, and the degrees corresponding to the directions of several particle collectors increase in turn anti-clockwise), and the metal wall is a copper plane with a thickness of 1 cm located at the origin of the coordinates, which is placed 3 m away from the collectors. When the metal wall is striked by a bunch of 13.6 MeV gamma beams, which contains one million photons, secondary electrons can be produced. In our model, the secondary electrons are characterized by two parameters: the number and the average energy, which are recorded by the collectors.

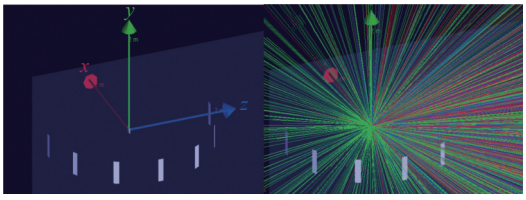

Fig. 4 Model of gamma rays stimulating metals to generate secondary ions in Monte Carlo, where the red, green and blue coordinate axes are the x-axis, y-axis and z-axis respectively

Fig. 5a shows the number of scattering secondary electrons in different angles when the gamma rays strike the copper plane. The angle between gamma rays and the normal line of the copper plane defines the incident angle of gamma. The angles in x-z axis denote the location of collectors.

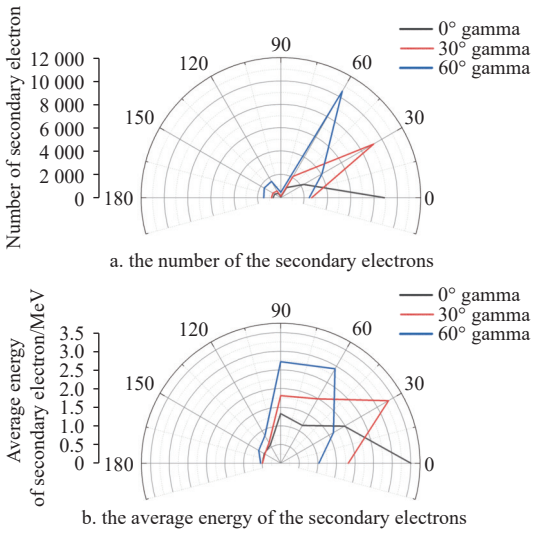

Fig. 5 Scattering secondary electrons in different directions when gamma rays hit copper planes

It can be seen that the number of secondary electrons reaches a maximum value when the angle of gamma ray overlaps with the angle of collector, suggesting that the collector is lined up with gamma rays, where the number of secondary electrons is remarkably reduced with the angle of collectors. The minimum number of secondary electrons emerges at the orthogonal view. As a good conductor, the copper plane can accommodate a huge amount of free electrons, which can interact with energetic photons to generate hot electrons[26]. This reaction is described by the rate equation:

$$\frac{\mathrm{d}n_2}{\mathrm{d}t} = Kn_1(n_2+1)N_1 - Kn_2(n_1+1)N_2 \tag{1}$$

Here n_1 refers to the number of incident photons, n_2 the number of scattered photons, K is a constant determined by the scattering cross section, N_1 the number of electrons in the emis-sion process and N_2 the number of electrons in the absorption process. $Kn_1(n_2+1)N_1$ represents the generation of electrons in the emission and $Kn_1(n_2+1)N_1$ means the loss of electrons in the absorption process. Once the electrons emit from the plane, photons continue to interact with hot electrons[27]. Most of the electrons are collected in the incident direction of gamma ray, indicating that most secondary electrons are generated at the orientation of gamma ray.

When gamma rays hit the copper plane from different directions, secondary electrons surrounding the plane achieve varying average energies as shown in Fig. 5b. Secondary electrons are more energetic at the direction of gamma ray. Afterwards, the average energy of secondary electrons drops by enlarging the angle of collector. The results imply that the energy of secondary electrons is closely related to the direction of gamma's injection. Meanwhile, most of the secondary electrons are collected in this direction, suggesting the energy deposition of secondary electrons is centralized at the direction of gamma incidence and the primary flow direction of secondary electron.

Given that there are some diagnostic instruments having the aluminum outer wall, we also investigate the secondary electron during the gamma ray interacting with aluminum as displayed in Figs. 6a and 6b. In general, aluminum wall shows the same tendency in emission of secondary electron and its average energy is similar to that from copper, but electrons can hardly be found at the gamma incident side (collected at above 90 degrees). Considering all the settings are identical in the copper case, the results are thus determined by aluminum in nature. Furthermore, electrons derived from aluminum are fewer than those from copper, but the average energy is higher.

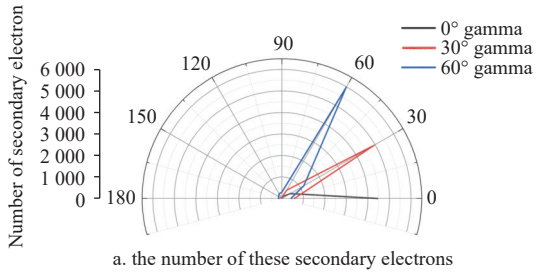

a. the number of these secondary electrons

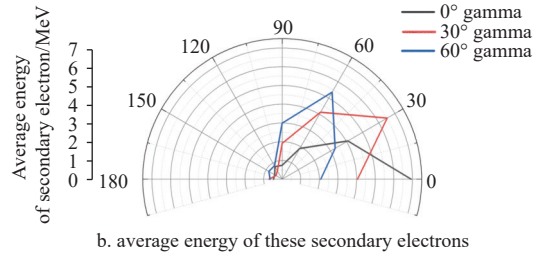

b. average energy of these secondary electrons

Fig. 6　Secondary electrons in different directions when gamma rays hit aluminum plane

To deepen understanding on the distinction between copper plane and aluminum plane, the gamma rays are injected along the normal line on the metal walls (Aluminum and Copper) with different thicknesses. As presented in Figs. 7a and 7b, the number of secondary electrons is significantly affected by the thickness of the plane, while the average energy of secondary electrons decreases with the thickness. Fig. 7c clearly shows the deviation of total energy deposition of electrons between copper and aluminum. Generally, more energies are converted to electrons during copper-gamma interactions than aluminum-gamma interaction when the metal wall is thinner than 1 cm. More energies are gained by electrons in aluminum than in copper when thickness is further enlarged, which mainly originates in the decline of the production of secondary electrons in copper. Furthermore, total energy deposition of electrons rapidly increases ranging from 0～10 mm, which reveals that energy transfers from gamma ray to secondary electrons at the outer part of metal.

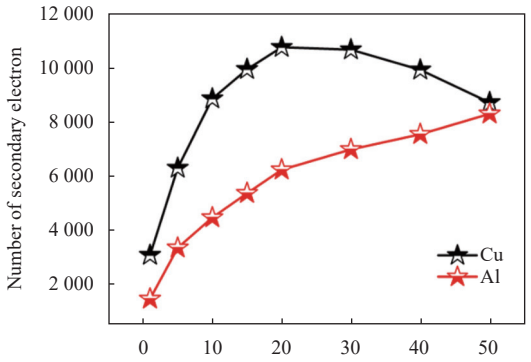

a. The number of secondary electrons as a function of metals' thickness

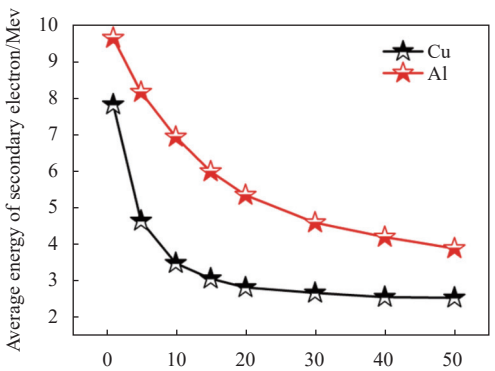

b. Evolution of average energy of secondary electrons with the thickness

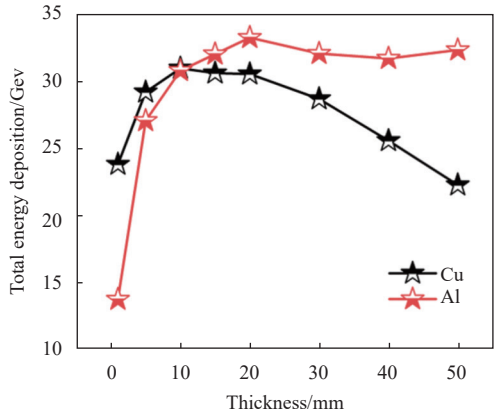

c. Variation of total energy deposition of secondary electrons

Fig. 7 The calculated number and energy of secondary eletrons with different metal thickness

Moreover, the effects of different metal shapes on the electrons are studied as shown in Fig. 8, where it can be seen that more emitted electrons are generated when gamma rays focus on a metal corner, but the average energy is the lowest. Besides, the number of secondary electron generated at the spherical surface is the minimum, while their average energy is the highest. Therefore, a conclusion can be drawn that when the energy of gamma ray remains constant, the number of emitted electrons is negatively correlated with its average energy.

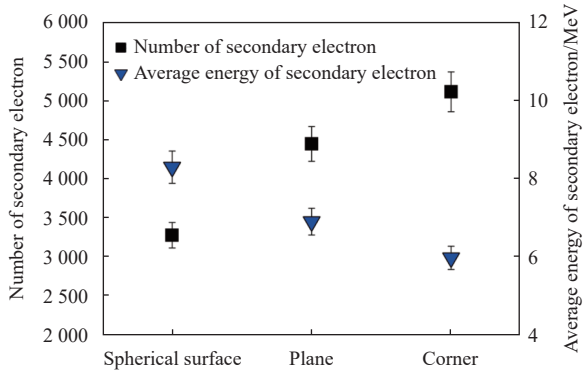

Fig. 8 The number and average energy of electrons generation stemming from different metal shapes

Positive charges tend to gather on surface of metal when electrons are flushed out. Besides, the metal potential depends rarely on the metal materials[19]. To gain the insight into the effects of metal shapes on the ejected secondary electrons, a Multiphysics model is thus constructed to verify the results. Fig. 9a indicates the corner between two mental flats is likely to gain a large number of positive charges. When the distribution of charges on sphere is balanced as shown in Fig. 9b, thepotential of sphere is larger than that of a flat metal, but it is lower than a metal corner. Intensities of electric field on different shapes provide different attractions between the surfaces and the secondary electrons, and the energy loss occurs to these escaping electrons affected by positive charges, which is reasonable for variations of the emitted electrons from different shapes of the metal surfaces.

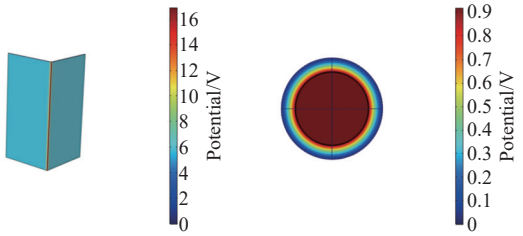

a. Distribution of charges on plane and corner b. Distribution of charges on sphere

Fig. 9 Distribution of charge at different positions

3 Conclusions

Gamma rays generated from the interaction between powerful lasers and solid targets can interact with metal to generate secondary electrons, which induces secondary EMP radiations. A model combined with Monte Carlo and multiphysics model is developed in this study. Energy spectra and spatial distributions of secondary electrons are revealed. The results indicate that most energy of the secondary electrons gathers near the direction of the incident gamma rays, and more electrons with lower average energy are produced from a thicker metal wall. The shape of the metal strongly affects the generation of secondary electrons. Negative correlations are found between average energy and numbers in shapes. The resulting conclusions are beneficial to deeply understand the EMP generation during the power laser shooting targets and to the shielding design on some precious diagnostic setups.

References

[1] LINDL J. Development of the indirect - drive approach to inertial confinement fusion and the target physics basis for

ignition and gain[J]. Physics of Plasmas, 1995, 2(11): 3933-4024.
[2] CAMPBELL E M, GONCHAROV V N, SANGSTER T C, et al. Laser-direct-drive program: Promise, challenge, and path forward[J]. Matter and Radiation at Extremes, 2017, 2(2): 37-54.
[3] ZHENG W, WEI X, ZHU Q, et al. Laser performance upgrade for precise ICF experiment in SG-Ⅲ laser facility[J]. Matter and Radiation at Extremes, 2017, 2(5): 243-255.
[4] FLEUROT N, CAVAILLER C, BOURGADE J L. The laser megajoule (LMJ) project dedicated to inertial confinement fusion: Development and construction status[J]. Fusion Engineering and Design, 2005, 74(1-4): 147-154.
[5] BROWN JR C G, AYERS J, FELKER B, et al. Assessment and mitigation of diagnostic-generated electromagnetic interference at the National Ignition Facility[J]. Review of Scientific Instruments, 2012, 83(10): 10D729.
[6] ALVAREZ J, RIVERA A, GONZALEZ-ARRABAL R, et al. Materials research for HiPER laser fusion facilities: chamber wall, structural material and final optics[J]. Fusion Science and Technology, 2011, 60(2): 565-569.
[7] MACGOWAN B J, DA SILVA L B, FIELDS D J, et al. Short wavelength x-ray laser research at the Lawrence Livermore National Laboratory[J]. Physics of Fluids B: Plasma Physics, 1992(4): 2326.
[8] MINIATI F, JONES T W, KANG H, et al. Cosmic-Ray electrons in groups and clusters of galaxies: Primary and secondary populations from a numerical cosmological simulation[J]. The Astrophysical Journal, 2001, 562(1): 233.
[9] POVARNITSYN M E, ROSMEJ O N, ANDREEV N E. On ionization dynamics of metal targets irradiated by high-contrast relativistic-intense laser pulses[J]. Journal of Physics: Conference Series, 2019, 1147(1): 012079.
[10] LI X F, L'HUILLIER A, FERRAY M, et al. Multiple-Harmonic generation in rare gases at high laser intensity[J]. Physical Review A, 1989, 39(11): 5751.
[11] GABICI S, AHARONIAN F A. Gamma ray signatures of ultra high energy cosmic ray accelerators: electromagnetic cascade versus synchrotron radiation of secondary electrons[J]. Astrophysics and Space Science, 2007, 309(1): 465-469.
[12] LONGMIRE C L. On the electromagnetic pulse produced by nuclear explosions[J]. IEEE Transactions on Electromagnetic Compatibility, 1978(1): 3-13.
[13] YEE J H, ALVAREZ R A, MAYHALL D J, et al. Theory of intense electromagnetic pulse propagation through the atmosphere[J]. The Physics of Fluids, 1986, 29(4): 1238-1244.
[14] BRADFORD P, WOOLSEY N C, SCOTT G G, et al. EMP control and characterization on high-power laser systems[J]. High Power Laser Science and Engineering, 2018, 6: e21-e28.
[15] HJALMARSON H P, MAGYAR R J, CROZIER P S, et al. Physics of intense, high energy radiation effects[R]. Funding Organisation: US Department of Energy (United States), 2011.
[16] POYÉ A, HULIN S, BAILLY-GRANDVAUX M, et al. Physics of giant electromagnetic pulse generation in short-pulse laser experiments[J]. Physical Review E, 2015, 91(4): 043106.
[17] RADASKY W A, BAUM C E, WIK M W. Introduction to the special issue on high-power electromagnetics (HPEM) and intentional electromagnetic interference (IEMI)[J]. IEEE Transactions on Electromagnetic Compatibility, 2004, 46(3): 314-321.
[18] DE MARCO M, PFEIFER M, KROUSKY E, et al. Basic features of electromagnetic pulse generated in a laser-target chamber at 3-TW laser facility PALS[J]. Journal of Physics: Conference Series, 2014, 508(1): 012007.
[19] YANG M, LI T, WANG C, et al. Characterization of electromagnetic pulses via arrays on ShenGuang-III laser facility laser[J]. Chinese Optics Letters, 2016, 14(10): 101402.
[20] ZHENG W, WEI X, ZHU Q, et al. Laser performance of the SG-III laser facility[J]. High Power Laser Science and Engineering, 2016, 4:
[21] HU D, DONG J, XU D, et al. Generation and measurement of complex laser pulse shapes in the SG-III laser facility[J]. Chinese Optics Letters, 2015, 13(4): 041406.
[22] YI T, YANG J, Yang M, et al. Investigation into the electromagnetic impulses from long-pulse laser illuminating solid targets inside a laser facility[J]. Photonic Sensors, 2016, 6(3): 249-255.
[23] YANG M, YANG Y, LI T, et al. Electromagnetic radiations from laser interaction with gas-filled Hohlraum[J]. Laser Physics Letters, 2017, 15(1): 016101.
[24] YANG J W, LI T S, YI T, et al. Measurement and analysis of electromagnetic pulse from laser-target interaction at ShenGuang II laser facility[J]. Fusion Science and Technology, 2017, 72(1): 41-48.
[25] DUBOIS J L, LUBRANO-LAVADERCI F, RAFFESYIN D, et al. Target charging in short-pulse-laser–plasma experiments[J]. Phys Rev E, 2014, 89(1): 013102-013116.
[26] PANTELL R, SONCINI G, PUTHOFF H. Stimulated photon-electron scattering[J]. IEEE Journal of Quantum Electronics, 1968, 4(11): 905-907.
[27] CHEN P, DAWSON J M, HUFF R W, et al. Acceleration of electrons by the interaction of a bunched electron beam with a plasma[J]. Physical Review Letters, 1985, 54(7): 693.

编　辑　叶　芳